Proceedings of ASME Turbo Expo 2025
Turbomachinery Technical Conference and Exposition
GT2025
June 16-20, 2025, Memphis, Tennessee

GT2025-151884

METHODOLOGY FOR EXPLORING SOFC SYSTEM LAYOUTS IN A HIGHLY INTEGRATED HYBRID PROPULSION SYSTEM

Luca Mantelli
University of Genoa
Genova, Italy

Abhishek Dubey
University of Genoa
Genova, Italy

Dario Buzzola
University of Genoa
Genova, Italy

Mario L. Ferrari
University of Genoa
Genova, Italy

Evangelia Pontika
Cranfield University
Cranfield, UK

Stefan Kazula
German Aerospace Center (DLR)
Cottbus, Germany

Daniel Ewald
Karlsruhe Institute of Technology
Karlsruhe, Germany

Andre Weber
Karlsruhe Institute of Technology
Karlsruhe, Germany

Stefanie De Graaf
German Aerospace Center (DLR)
Cottbus, Germany

ABSTRACT

This paper presents a methodology to compare different layouts of a solid oxide fuel cell (SOFC) system, focusing on component integration and constraints for low-emission aircraft propulsion. The SOFC system is a subsystem of an Integrated Power and Propulsion System (IPPS) fueled by hydrogen and tightly coupled with a micro gas turbine (mGT). The methodology presented here is applied to the case study of a mGT-SOFC and will later help to define the SOFC system layout for the 1MW+ IPPS of the FlyECO project.

Due to the low power density of current SOFCs designed for stationary applications, technology projections are used to explore a scenario of entry into service in 2050. Parametric analyses have been performed to consider possible future developments and performance opportunities on the basis of anticipated increases in SOFC power density, which so far could only be implemented on a laboratory scale.

Different SOFC system layouts are defined by assuming different aircraft operating conditions (take-off and cruise) as design point, due to the important impact of ambient pressure and temperature in-flight variation on the SOFC system, the related components and the overall performance. To maximize the synergy between SOFC and mGT, all layouts are based on a pressurized SOFC and include a heat exchanger for heat recovery and flow pre-heating.

The system performance exploration is carried out with the W-TEMP software, varying the hybridization factor of the mGT-SOFC system between 5% and 20%, and comparing its performance to a baseline H_2-fueled mGT. The results obtained for this performance exploration report details on the coupling aspects between the micro gas turbine and the SOFC system and show clearly the advantages of mGT-SOFC integration in terms of net efficiency and production of water, which can be used in the combustion chamber of the mGT to limit the formation of NO_x. In conclusion, a procedure to preliminary estimate the mass of the main components in each layout is also presented, to assess how different choices in the design of the mGT-SOFC can affect its weight.

Keywords: SOFC, Hybrid system, Propulsion, Aviation

NOMENCLATURE

Symbols

A_{cell}	*total cell area*
Bi_{met}	*Biot number of turbine blade metal*
Bi_{TBC}	*Biot number of thermal barrier coating*
F	*Faraday constant*
I_{cell}	*cell current*
ε_o	*cooling effectiveness*
ε_f	*film cooling effectiveness*
J	*current density*
K_{cool}	*cooling flow factor*
LHV	*lower heating value*
m	*mass*
$\dot{m}$	*mass flow rate*
n	*number of electrons involved in the reaction*
N	*number of compressor/turbine stages*

p	*pressure*
P	*power*
$P_{specific}$	*specific power*
p_X	*partial pressure of each substance X*
Q	*heat*
R	*gas constant*
S	*non-dimensional sensitivity*
T	*temperature*
t	*thickness of the heat exchanger*
TET	*turbine entry temperature*
UF	*utilization factor*
U_g	*Gibbs potential*
V_{Nernst}	*Nernst voltage*
V_{real}	*real voltage*
β	*pressure ratio*
Δp	*pressure loss*
ΔV_{act}	*activation overvoltage*
ΔV_{conc}	*concentration overvoltage*
ΔV_{ohm}	*ohmic overvoltage*
x	*model input*
y	*model output*
η_{CC}	*combustion efficiency*
η_{net}	*net efficiency*
η_{poly}	*polytropic efficiency*
η_{SOFC}	*SOFC efficiency*
η_{int}	*internal convective cooling efficiency*
Ψ	*cooling flow ratio*

Subscripts

amb	*ambient*
adwall	*adiabatic wall temperature*
an	*anode*
bl	*blade*
C	*compressor*
cat	*cathode*
ca	*cooling air*
g	*main gas flow in turbine*
in	*inlet*
nom	*nominal*
out	*outlet*
T	*turbine*
tot	*total*

Acronyms

AC	*auxiliary compressor*
CC	*combustion chamber*
DOH	*degree of hybridization*
EM	*electric motor*
EV	*expansion valve*
GB	*gearbox*
HB	*hybrid system*
HEX	*heat exchanger*
IPPS	*integrated power and propulsion system*
mGT	*micro gas turbine*
OPR	*overall pressure ratio*
PMDS	*power management & distribution system*
PEMFC	*polymeric exchange membrane fuel cell*
PR	*propeller*
SOFC	*solid oxide fuel cell*
W-TEMP	*web thermoeconomic modular program*

1. INTRODUCTION

Considering the climate-neutral target related to the aviation sector [1], innovative propulsion technology must be proposed for the coming decades. This is essential to obtain a carbon-neutral economy despite a forecasted scenario with significant passenger traffic increase [2]. Current research activities are proposing systems based on electrification, ranging from hybrid solutions [3] to full-electric propulsion systems [4].While the hybridization of fossil-fuel-based systems is not able to eliminate the in-flight CO_2 emissions, a fully battery-based propulsion system is subject to important constraints in terms of range and/or payload [5]. For this reason, attention is also focused on hydrogen-based propulsion to join high energy density (especially with liquid hydrogen [6] or other carbon-free chemicals such as ammonia [7]) with zero CO_2 emissions. Although traditional gas turbines fueled by hydrogen are proposed [8], application of fuel cell technology is considered a promising solution for producing significant efficiency increase in regional aircraft [9].

The application of fuel cells in aircrafts for non-propulsive power is not a new concept. For instance, Polymeric Exchange Membrane (PEM) fuel cells integrated with turbocharger technology [10] and SOFCs coupled with gas turbines are proposed in different layouts for auxiliary power unit applications [11]. However, the development of low-emission aircraft concepts activated interest in propulsion systems based on fuel cells, starting from PEM technology. For instance, due to the high power density performance of PEMs, it was possible to increase the specific energy from 0.2 kWh/kg (with commercial LiPo batteries) to 0.51 kWh/kg with an H_2-fueled system equipped with PEM technology [12]. Moreover, further activities considered PEM fuel cells for aircraft propulsion (e.g. converting a battery-based system [13] or optimizing the operating conditions [14]). Regarding the application of fuel cell

technology for aircraft propulsion, attention was also focused on SOFCs due to high efficiency performance and extended lifetime for stationary applications (50,000 h against 30,000 h for PEMFCs [15]). So, despite lower power density and additional constraints [16] (in comparison to PEMs), different authors analyzed SOFC-based systems for aircraft propulsion, ranging from fuel processing technology [17] to applications for unmanned aerial vehicles [18].

Considering the performance (mainly very high efficiency and low emissions) obtained with different studies on SOFCs integrated with gas turbines [19] or turbochargers [20], attention started to be focused on such hybrid systems for aircraft propulsion too [21]. Moreover, given the minor impact of manufacturing (2.1-9.5%) and disposal (0.1–0.6%) on the life cycle emissions of SOFCs fueled with natural gas, the direct use of hydrogen could be particularly effective to reduce the environmental impact of the aviation sector. Within this context, the ongoing FlyECO Horizon Europe project [22] aims to develop a 1 MW+ IPPS fueled by hydrogen, taking into account component integration and constraints [23].

This paper presents the methodology to design, simulate and analyze a H_2-fueled mGT-SOFC system for aviation, considering, as preliminary case study, a system with nominal power target of ~955 kW at take-off and ~410 kW at cruise. The performance of components included in the mGT-SOFC is assumed to be consistent with a future entry into service in 2050. This procedure will later help to define the SOFC system layout for the 1MW+ IPPS of the FlyECO project.

2. MOTIVATION AND CASE STUDY

The target of this paper is to define and present a methodology to design, analyze and compare different layouts of an mGT-SOFC system for aircraft propulsion.

2.1. Motivation

Given the necessity to develop a high efficiency and low emission propulsion system, the mGT-SOFC technology is considered a promising option, thanks to the synergy between mGT and SOFC. In fact, the performance of the fuel cell is enhanced by the air pressurization by the mGT air compressor and, at the same time, the high temperature of the SOFC off-gases makes it possible to have a significant energy recovery in the turbine [24]. Moreover, the use of a fuel system based on liquid hydrogen is well aligned with the current decarbonization goals of the EU, thanks to its zero CO_2 emissions. Since the paper is focused on the mGT-SOFC system, the analysis on the hydrogen production [25] and the liquid hydrogen on-board storage and distribution system [26] is not part of this work.

Due to the mGT-SOFC application in an aircraft, the weight of the additional components (SOFC, heat exchangers, etc.) must be carefully considered. Regarding the SOFC stack, it is important to highlight that the technology available for stationary applications is not sufficient due to gravimetric power density in the range of 0.1 kW/kg [27]. Neither a 2030 target of 0.65 kW/kg [28] is reasonable for such a high power application. For instance, with 0.65 kW/kg of SOFC power density, a hybrid system with a 500 kW stack includes an additional weight of almost 770 kg. So, considering the other BoP devices to be installed (mainly heat exchangers, pipes and valves), it is easy to exceed 1 ton of additional weight. However, due to recently interest in light-weight applications, SOFC technology researchers proposed new solutions, such as reaching 2 kW/kg with the microtubular geometry (at cell level) [29] or 4.6 kW/kg with the monolithic design (at stack level) [30]. For this reason, mGT-SOFC systems could be further developed and pushed to meet aviation requirements. This paper proposes a methodology to explore solutions at SOFC system level with different SOFC sizes, expecting that the application of this technology will become acceptable in aircrafts in case of positive development and commercialization of such high-power density technology.

2.2. Case Study

Different layouts of an mGT-SOFC system for aircraft propulsion were considered as case study to demonstrate the proposed methodology. Due to the benefits of SOFC pressurization, atmospheric layouts or solutions with a fuel cell operating at an intermediate pressure were discarded. Also SOFC air pre-heating solutions based on an ejector were considered not suitable due to low flexibility (and controllability) of this component in the continuous dynamic conditions during a flight (significant change in ambient conditions and power/thrust requirement). While referring to a hydrogen-fueled mGT as baseline system, the following different options were explored:

- **The design point**: take-off (full power of ~955 kW and sea-level ambient conditions) or cruise (reduced power of ~410 kW and ambient conditions corresponding to an altitude of ~7600 m).
- **The strategy to balance the pressures** of SOFC subsystem and mGT at the combustor inlet: by further pressurizing the SOFC with an auxiliary compressor (AC) or by reducing the pressure on the mGT air line with an expansion valve (EV). The first hybrid layout is here referred to as HB-1, while the second one as HB-2.

Figure 1, Figure 2 and Figure 3 show the differences between the baseline mGT and the proposed layouts. In these figures, air flows are in blue, hydrogen flows are in orange, cathode and anode outlet flows are in green and red, respectively, and combustion chamber exhausts are in purple. The SOFC system, which is the focus of this design procedure, is highlighted in orange.

In all the mGT-SOFC layouts, the air flow extracted at compressor outlet is pre-heated with a counter-flow heat exchanger (HEX) that exploits the high temperature of SOFC exhausts at the cathodic side. The fuel (hydrogen) should be preheated with a devoted system before entering the anode of the SOFC. However, due to the low amount of heat required for the fuel pre-heating (due to fuel low mass flow rate), its impact is

considered quite negligible in terms of the global calculations (e.g. system efficiency) and additional weight. For this reason, this component is neglected in the present methodology and the fuel flow is assumed to be at the desired temperature. The fuel should also be provided at the same pressure as the cathode flow to avoid pressure gradients in the SOFC. The SOFC exhausts (both anode and cathode outlet flows) are finally mixed in the micro gas turbine burner, where additional hydrogen is injected.

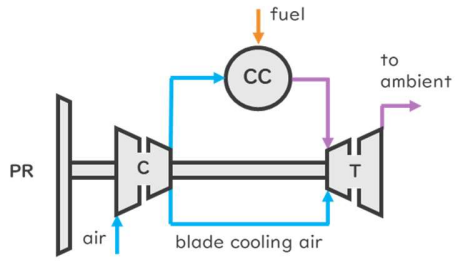

Figure 1: Baseline mGT plant layout.

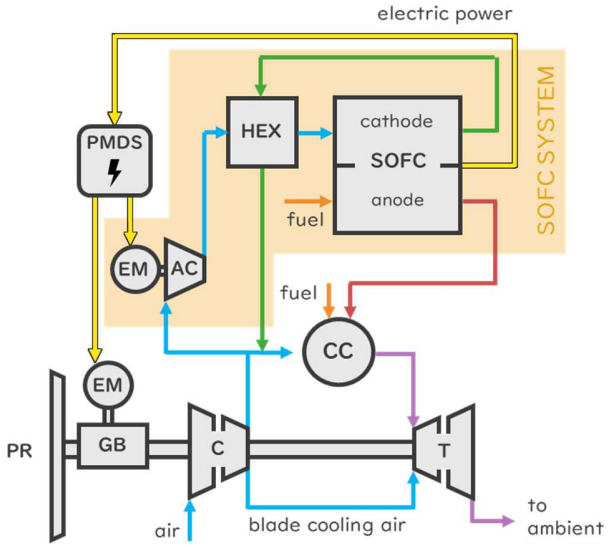

Figure 2: HB-1 plant layout (mGT-SOFC system with auxiliary compressor).

It is important to highlight that the steam produced by the SOFC is useful here for the containment of the NO_x emissions [31]. The electrical power output of the SOFC is regulated by a power management and distribution system (PMDS) to integrate the SOFC system with the other subsystems in the IPPS. In all the mGT-SOFC layouts considered, the SOFC power output is used to drive an electric motor connected to a gearbox (GB) installed on the mGT shaft, providing part of the mechanical power necessary for propulsion and increasing the efficiency of the system. However, this integration is specific of this case study. The same methodology could be easily extended to analyze different IPPS solutions.

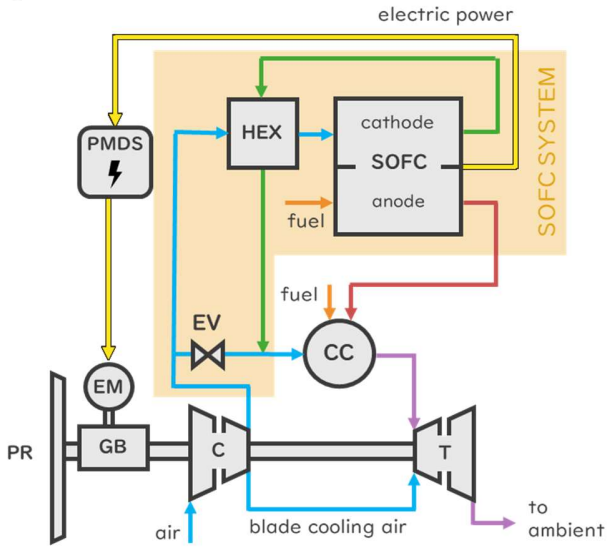

Figure 3: HB-2 plant layout (mGT-SOFC system with expansion valve).

3. METHODOLOGY

3.1. W-TEMP simulation software

The simulations presented and discussed in this paper were carried out with the software by the University of Genoa, named Web ThermoEconomic Modular Program (W-TEMP) (it is the tool that in [32] was named Widget-TEMP). It is an in-house visual modular program developed during the past 30 years for simulating the design of energy systems ranging from traditional to advanced plants. W-TEMP is able to perform thermodynamic, economic and exergetic analyses of a large number of power plants with more than 90 validated component modules [32]. For the thermal point of view, operating characteristics and mass and energy balances of each component are calculated sequentially in design conditions. While this work focuses attention only on the thermodynamic part to evaluate the mGT-SOFC performance exploration, no further details are discussed on the economic and exergetic sides.

For the components related to the mGT (compressor, combustor, turbine and electrical generator), an early validation was performed in [32] obtaining errors lower than 1% from the thermodynamic point of view. Moreover, the SOFC stack was validated in [24] obtaining errors in the 1.6%-8.0% range for the voltage and in the 1.1%-4.9% range for the temperature. It was considered a good performance due to the comparison with results obtained in different previous works, such as an early computational fluid dynamic analysis on the SOFC stack reported in [33]. The simulation results obtained with an early version of the W-TEMP tool (named simply TEMP) were able to validate the software also at plant level including further components, such as the recuperator. As reported in [24], the

error values related to the system global efficiencies were lower than 0.8%. Finally, it is important to show that the models of the components included in this work were used also in more recent activities related to liquid fuel-based SOFC hybrid systems [34] and applications in aircrafts [35].

3.2. SOFC Model

The SOFC model was previously developed by Massardo and Lubelli for the simulation of solid oxide fuel cells with or without internal reforming [24]. The electrochemical oxidation of hydrogen (Eq. (1)) is simulated based on the available mass flow and its utilization factor.

$$2H_2 + O_2 \rightarrow 2H_2O \tag{1}$$

The voltage of the SOFC is evaluated starting from the Nernst voltage V_{Nernst} (Eq. (2)):

$$V_{Nernst} = U_g + \frac{RT}{nF} \cdot ln\left(\frac{p_{H_2} \cdot p_{O_2}^{1/2}}{p_{H_2O}}\right) \tag{2}$$

Where U_g is the Gibbs potential, R is the gas constant, n is the number of electrons involved in the electrochemical reaction, F is the Faraday constant and p_X represents the partial pressure of each substance X.

The real voltage V_{real} is then obtained by subtracting the activation, ohmic and concentration losses from V_{Nernst} (Eq. (3)).

The activation overpotential is estimated as proposed by Aguiar et al. [36], using the Butler–Volmer equation, opportunely corrected to take into account the effect of charge and mass transfers. Ohmic losses are obtained from the electrical resistance R_{ohm} following the approach by Bessette [37] (Eq. (4)). Resistivities ρ of cathode electrode, electrolyte and anode electrode are computed separately as functions of temperature T (Eq. (5)) and coefficients α and β which are specific of the material.

$$V_{real} = V_{Nernst} - \Delta V_{act} - \Delta V_{ohm} - \Delta V_{conc} \tag{3}$$

$$R_{ohm} = \rho\, L\, /A \tag{4}$$

$$\rho = \alpha\, e^{\beta/T} \tag{5}$$

The electrode polarization effect is modeled as proposed by Achenback [33], using Eqs. (6) and (7)

$$\frac{1}{R_{pol,cat}} = K_{cat} \cdot \frac{4F}{RT}\left(\frac{p_{O_2}}{p_{ref}}\right)^m e^{-(E_{act,cat}/RT)} \tag{6}$$

$$\frac{1}{R_{pol,an}} = K_{an} \cdot \frac{2F}{RT}\left(\frac{p_{H_2}}{p_{ref}}\right)^m e^{-(E_{act,an}/RT)} \tag{7}$$

where R_{pol} is the electrical resistance corresponding to the polarization effect, K and m are empirical coefficients, p_{ref} is a reference pressure and E_{act} is the activation overpotential.

It must be noted that the computation of all voltage losses relies on the value of cell temperature, which is not initially known. This temperature is obtained by satisfying the conservation equation and implementing a bisection method [24].

The power output P_{SOFC} is obtained as the product of real voltage V_{real}, current density J and total cell area A_{cell} (Eq. (8)). Finally, the SOFC efficiency is determined with Eq. (9), where LHV_{H2} is the lower heating value of hydrogen and $\dot{m}_{H2}$ is its mass flow.

$$P_{SOFC} = V_{real} \cdot J \cdot A_{cell} \tag{8}$$

$$\eta_{SOFC} = \frac{P_{SOFC}}{LHV_{H_2} \cdot \dot{m}_{H_2}} \tag{9}$$

Within W-TEMP, current density, oxygen and hydrogen excess ratios (UF_{O2} and UF_{H2}, respectively) are set by the user. Based on the inlet flows and current density, the model computes the composition and temperature of the outlet flows, the efficiency, voltage and power, as well as the fuel cell area to be installed to achieve the desired performance. The SOFC model was calibrated to match the performance of the stack presented by Massardo and Lubelli [24]. The same study verified the accuracy of the W-TEMP SOFC model when used to simulate mGT-SOFC hybrid systems by replicating the performance of the system proposed by Harvey and Richter [38].

3.3. mGT Model

The mGT is modelled in WTEMP relying on compressor and turbine modules, which can be used to simulate turbomachinery of various sizes, from small mGTs to large heavy-duty gas turbines. All simulations in this work are performed considering the characteristics of an mGT and assuming turbine cooling. Each turbine stage consists of a stator and rotor row. The cooling flow ratio is separately calculated for stator or rotor. In the first step, the stator cooling air is mixed with the main gas flow, and the resulting mixture is expanded in the rotor [39,40]. A mixing pressure loss equal to 0.07 Ψ (where Ψ is the cooling flow ratio) was considered for the mixing of the main gas flow and cooling flow in the stator based on the correlation developed by Horlock et al. [41].

The cooling flow is estimated as per the model developed by Wilcock et al. [42]. It predicts cooling flow ratio (Ψ) based on different cooling technology levels expressed in terms of five parameters (Eqs. (10)-(14)), namely cooling flow factor (K_{cool}), internal convective cooling efficiency (η_{int}), film cooling effectiveness (ε_f), Biot number of turbine blade metal (Bi_{met}) and Biot number of thermal barrier coating (Bi_{TBC}). For a given main gas temperature (T_g), allowable blade metal temperature (T_{bl}) and cooling flow inlet temperature ($T_{ca,in}$), the cooling effectiveness (ε_o) is calculated by Eq. (10), and then, Ψ is estimated from Eq. (14) using the parameters listed in Table 1 for blade cooling model used in this work.

$$\varepsilon_o = \frac{(T_g - T_{bl})}{(T_g - T_{ca,in})} \quad (10)$$

$$\eta_{int} = \left(\frac{T_{ca,out} - T_{ca,in}}{T_{bl} - T_{ca,in}}\right) \quad (11)$$

$$\varepsilon_f = \left(\frac{T_g - T_{adwall}}{T_g - T_{ca,out}}\right) \quad (12)$$

$$Bi_{tot} = Bi_{TBC} - Bi_{met}\left(\frac{\varepsilon_o - \varepsilon_f}{1 - \varepsilon_o}\right) \quad (13)$$

$$\Psi = \frac{m_{ca}}{m_g} = \frac{K_{cool}}{(1 + Bi_{tot})}\left(\frac{\varepsilon_o - \varepsilon_f\,[1 - \eta_{int}(1 - \varepsilon_o)]}{\eta_{int}(1 - \varepsilon_o)}\right) \quad (14)$$

Table 1: Parameters of blade cooling model.

Parameter	Symbol	Value
Cooling flow factor	K_{cool}	0.045
Internal convective cooling efficiency	η_{int}	0.70
Film cooling effectiveness	ε_f	0.40
Biot number of blade metal	Bi_{met}	0.15
Biot number of thermal barrier coating	Bi_{TBC}	0.30

3.4. Evaluation of weights

Given the aeronautical application, the mGT-SOFC system will be beneficial only if its weight is not excessive to the point that it will increase the total energy consumption and NOx emissions due to the increased aircraft weight. Therefore, the proposed methodology does not focus only on the technical performance of the proposed layouts, but also on the weight of their main components, which are determined according to the methodology proposed by Collins and McLarty [43]. This study provides correlations of weights and values of power densities to estimate the contributions of SOFC, turbomachinery, heat exchangers and electric motors. The weight of other components, such as combustion chamber, ducts and electrical devices, are here neglected in this preliminary exploration and must be included in the future to achieve more accurate results.

The mass of the SOFC depends on the specific technology. As explained in Section 2.1, current commercial SOFCs are not suitable for aviation due to their low power density. Therefore, this analysis is based on the assumption that more innovative and lightweight SOFC will be available in the future. Including the mass of interconnects, seals, ceramic fiber insulation and a T-700 carbon fiber pressure vessel, the power density of a SOFC stack is assumed to be equal to 1.88 kW/kg for planar cells and to 4.60 kW/kg for monolithic cells. The masses of pressure vessel and insulation were determined based on Collins and McLarty [43] to withstand a stack pressure of 10 bar and to keep the vessel under 85°C (maximum temperature of T-700).

Compressor and turbine of the mGT are considered as machines with equal pressure ratios among the stages. Their mass is computed as a function of their number of stages N (4 compression stages and 2 expansion stages in total), inlet mass flows $\dot{m}_{in}$, pressure ratios β, according to Eqs. (15) and (16), which have been derived from the data reported in [44] following the approach of Collins and McLarty [43].

$$m_C = N\frac{\dot{m}_{in}}{1.16}(0.213\beta^2 - 2.51\beta + 16.9) \quad [kg] \quad (15)$$

$$m_T = N\frac{\dot{m}_{in}}{1.16}(-0.38\beta^2 + 5.5\beta + 1.19) \quad [kg] \quad (16)$$

The mass of the auxiliary compressor is also computed with Eqs. (15), considering it as a single stage machine. The mass of the heat exchanger is computed with Eq. (17) as a function of its area A, thickness t and solid density ρ. The area is automatically computed by W-TEMP to guarantee the proper SOFC inlet conditions, t is set equal to 1.8 mm and ρ to 2700 kg/m^3, according to [43]. as a function of its area A, thickness t and solid density ρ. The area is automatically computed by W-TEMP to guarantee the proper SOFC inlet conditions, t is set equal to 1.8 mm and ρ to 2700 kg/m^3, according to [43].

$$m_{HEX} = A \cdot t \cdot \rho \quad [kg] \quad (17)$$

Following the methodology presented in [43], a preliminary mass of electric motors is estimated assuming a power density of 24 kW/kg.

3.5. Simulation setup

The two different layouts of mGT-SOFC (HB-1 and HB-2) are designed by setting take-off (T_{amb} = 15°C, p_{amb} = 1.013 bar) or cruise (T_{amb} = -27°C, p_{amb} = 0.405 bar) as nominal point and compared with a hydrogen-fueled mGT capable of generating the same power under the same conditions. Systems designed for take-off are identified by the letter "T" and those designed for cruise by the letter "C".

The performance of the standalone mGT is assumed to be the same as the one integrated with the SOFC, and it is based on the parameters in Table 2. Since the mGT power split goes only from 100% to 80%, the polytropic efficiency of compressor and turbine was assumed to be constant among all layouts. Given the focus on future technologies of this explorative study, this value was set at 91%. Similarly, the HEX heat exchange coefficients are always kept equal for all configurations. Also for the standalone mGT, the value of T_{bl} was calibrated to keep the cooling bleed as 5% of the compressor flow.

The performance of the SOFC is based on the one previously analyzed by Massardo and Lubelli [24] for the validation of the W-TEMP model. For each simulation, the SOFC is assumed to work under the conditions reported in Table 3. Pressure losses are assumed to be equal to 1.5% across anode

and cathode of the SOFC, and equal to 1% across both channels of the HEX. These values were selected based on the authors' previous experience on SOFC hybrid systems [16,20].

All the performance parameters defined in this section are specific to the considered case study and could be easily modified to apply the same methodology to other IPPS, such as the 1 MW+ of the FlyECO project [23].

Table 2: Characteristic parameters of the mGT for this explorative case study.

	Take-off	Cruise
TET	1027°C	927°C
$p_{T,out}$	1.317 bar	0.527 bar
OPR	10	
η_{CC}	99.9%	
Δp_{CC}	4.0%	

Table 3: Operational parameters of the SOFC for this explorative case study.

I_{cell}	2400 A/m²
UF_{H2}	0.8
UF_{O2}	0.2
$T_{in,SOFC}$	725°C

Considering these parameters and assumptions, each mGT-SOFC system layout was simulated in W-TEMP for different degrees of hybridization (DOH), defined in this explorative activity as the percentage of total power generated by the SOFC. The performance of each layout is evaluated by its net efficiency, defined as Eq. (18):

$$\eta_{net} = \frac{P_T + P_{SOFC} - P_C - P_{AC}}{LHV_{H_2} \cdot (\dot{m}_{H_2,tot})} \quad (18)$$

where P_T is the power generated by the mGT turbines, P_C is the one consumed by the mGT compressor, P_{AC} is the one consumed by the AC (if present) and $\dot{m}_{H2,tot}$ is the total hydrogen mass flow (i.e., supplied to the cell and to the combustion chamber). The results of these simulations are analysed in the next section.

4. APPLICATION OF METHODOLOGY TO THE CASE STUDY

4.1. DOH Parametric analysis

Varying the DOH of the mGT-SOFC system between 5% and 20%, it is possible to observe how the performance of the hybrid systems changes, and to make a comparison with the baseline H_2 mGT. The results of the considered explorative case study show that all the mGT-SOFC systems have a higher net efficiency than the H_2 mGT, and that it increases almost linearly with the DOH, both for take-off and cruise conditions, as shown in Figure 4 and Figure 5. Among the configurations evaluated, the HB-1 layout demonstrates superior performance compared to the HB-2 in the explored case study. This is because the auxiliary compressor has low power consumption, whereas the valve reduces the system operating pressure, thereby compromising the efficiency of both the fuel cell and the micro gas turbine.

Despite the differences in efficiency shown in Figure 4 and Figure 5, at the current stage this methodology does not make it possible to draw conclusions regarding the best design condition (take-off or cruise). In fact, regardless of its design point, any layout will be required to operate both in take-off and cruise during a complete flight mission. During take-off, the system inlet pressure is significantly higher compared to cruise, allowing for increased pressurization. This condition enables the fuel cell to operate at higher performance levels, improving the net efficiency of the system, independently from its design condition. Therefore, the advantages of one design point over the other could be assessed only after an off-design analysis.

Since the overall power output of each plant (for cruise or take-off) is fixed, an increase in net efficiency directly leads to an equivalent decrease of fuel consumption. However, increase of DOH has also an effect on the additional hydrogen mass flow $\dot{m}_{H2,in,comb}$ that must be supplied to the combustion chamber of the mGT to reach the desired turbine inlet temperature $T_{T,in}$ (see Table 2). For higher DOHs, the hydrogen available in the anode off-gases increases. At the same time, the air mass flow of the mGT decreases, because it has to generate a lower percentage of the total power. These two effects combined lead to a decrease of $\dot{m}_{H2,in,comb}$ for both take-off and cruise, as shown in Figure 6 and Figure 7. The reduction of $\dot{m}_{H2,in,comb}$ is slightly more significant for the HB-1 layouts because of their higher net efficiency. For values of DOH < 5%, the efficiency of HB-2 would reach lower values than the mGT-C. This is mostly caused by the reduction of pressure at the turbine inlet having a negative effect on the performance of the system, which is more significant than the increase of efficiency thanks to the integration with the SOFC.

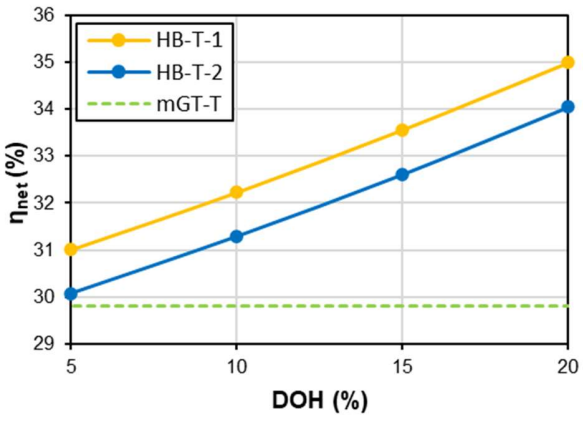

Figure 4: Relationship between thermodynamic efficiency (η_{net}) and degree of hybridization (DOH) for take-off (for this case study).

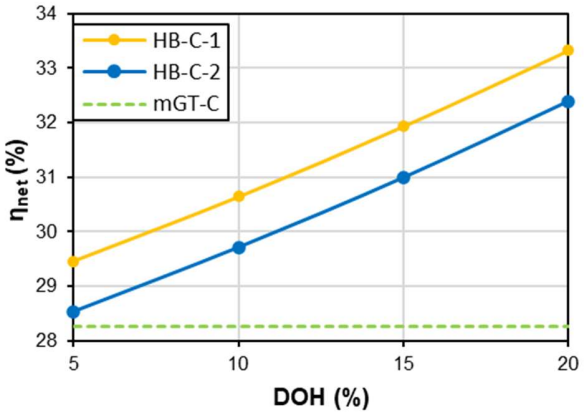

Figure 5: Relationship between thermodynamic efficiency (η_{net}) and degree of hybridization (DOH) for cruise (for this case study).

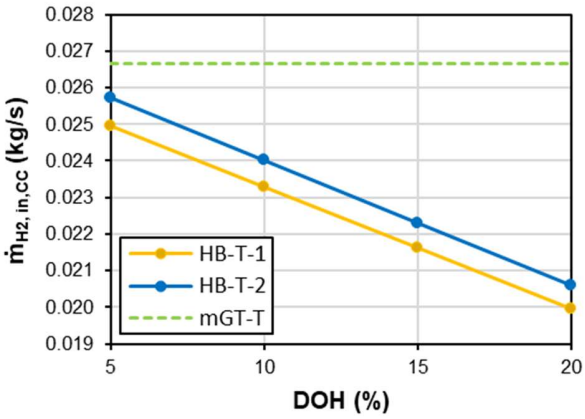

Figure 6: Relationship between H_2 combustion chamber inlet mass flow ($\dot{m}_{H2,in,CC}$) and degree of hybridization (DOH) for take-off (for this case study).

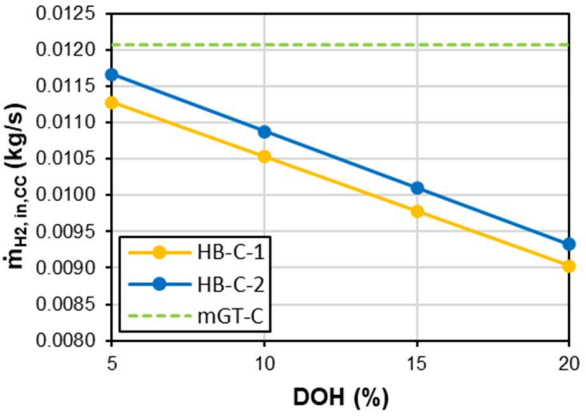

Figure 7: Relationship between H_2 combustion chamber inlet mass flow ($\dot{m}_{H2,in,CC}$) and degree of hybridization (DOH) for cruise (for this case study).

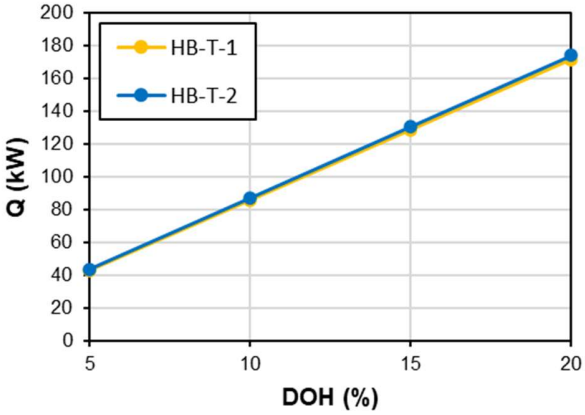

Figure 8: Relationship between heat exchanged by the HEX (Q) and degree of hybridization (DOH) for take-off (for this case study).

This parametric analysis also provides information that is useful to size the components of the mGT-SOFC system. For example, after fixing the heat losses and the effectiveness of the HEX necessary to reach the desired SOFC cathode inlet temperature $T_{in,SOFC,cat}$, the model computes the heat Q exchanged between the two flows. The SOFC is always assumed to be working with constant UF_{O2}, and the $T_{in,SOFC,cat}$ is fixed at 725°C. Thus, the cathode air flow grows linearly with the DOH, and so does the heat necessary to pre-heat it, with minimum differences between the HB-1 and HB-2 layouts as shown in Figure 8 and Figure 9.

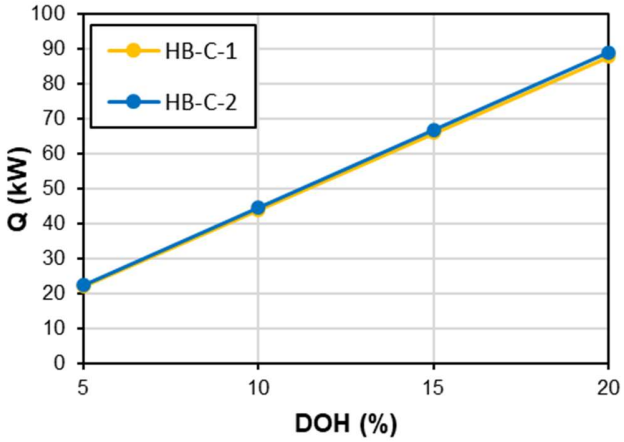

Figure 9: Relationship between heat exchanged by the HEX (Q) and degree of hybridization (DOH) for cruise (for this case study).

Specific power ($P_{specific}$) is a parameter that is defined as the ratio between generated power and air mass flow going through the mGT, often used in the analysis of gas turbines as a measure of their capability to obtain power from an air mass flow.

However, the SOFC generates electrical power by consuming the oxygen present in the air flow, and its operation is not based on a thermodynamic cycle. Therefore, it requires a much smaller air mass flow than a mGT to generate an equivalent power. For this reason, an increase of DOH leads to a remarkable growth of $P_{specific}$ (Figure 10 and Figure 11), which can exceed the one of the baseline mGT by more than 25% for a DOH of 20%. Also in this case, the performance of the HB-T is slightly better thanks to its higher efficiency.

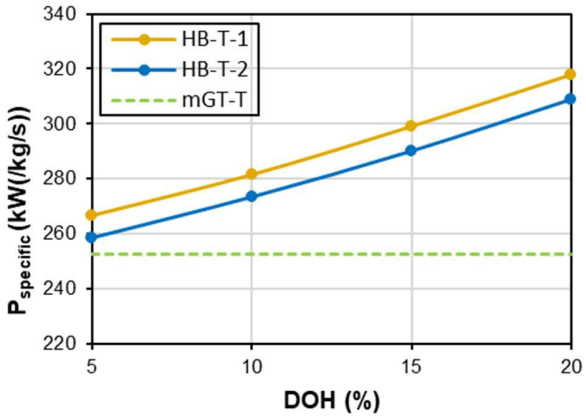

Figure 10: Relationship between specific power ($P_{specific}$) and degree of hybridization (DOH) for take-off (for this case study).

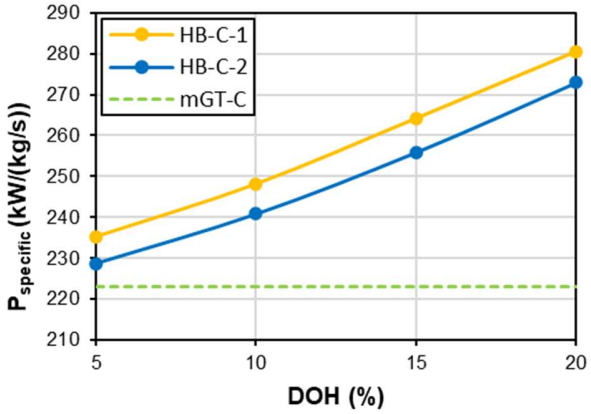

Figure 11: Relationship between specific power ($P_{specific}$) and degree of hybridization (DOH) for cruise (for this case study).

One of the advantages of integrating an SOFC with a hydrogen-fueled micro gas turbine, is the continuous supply of water steam from the anode off-gas. Burning hydrogen can lead to high temperatures and to the formation of NO_x when air is used for combustion. However, steam injection in the combustion chamber can limit excessive increases of temperature and prevent the creation of these pollutants [31]. As shown in Figure 12 and Figure 13, this steam flow increases linearly with the DOH, reaching a maximum for DOH=20% of about 19.7 g/s and 8.7 g/s for take-off and cruise, respectively. This corresponds to an injection in the combustion chamber of about 31.3 liters of water per hour of cruise flight, which should be stored onboard if the mGT were not integrated with the SOFC. Differences between HB-T and HB-C are minimal in this case, the steam production being directly related to the consumption of hydrogen in the SOFC.

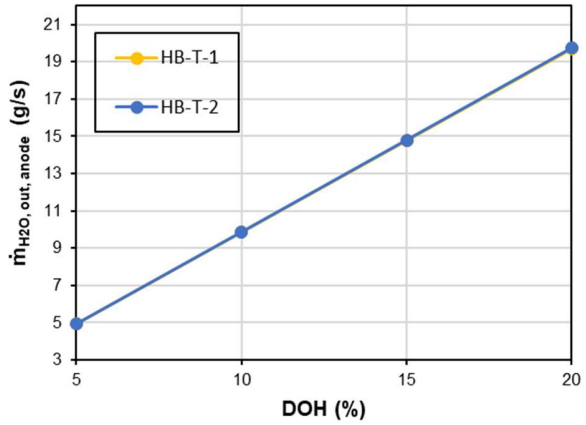

Figure 12: Relationship between H_2O at the inlet of the anode mass flow rate ($\dot{m}_{H2O,\ out,\ anode}$) and degree of hybridization (DOH) for take-off (for this case study).

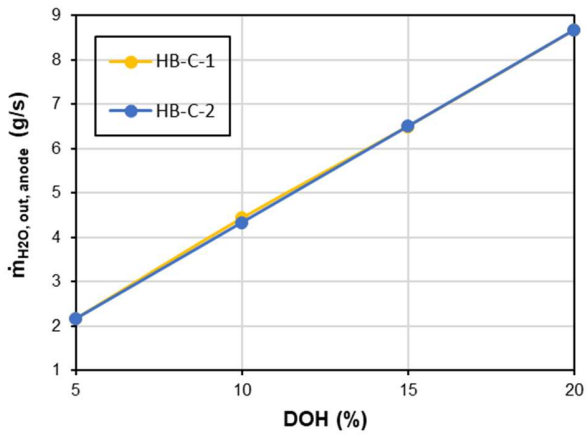

Figure 13: Relationship between H_2O at the inlet of the anode mass flow rate ($\dot{m}_{H2O,\ out,\ anode}$) and degree of hybridization (DOH) for cruise (for this case study).

4.2. Evaluation of weights

Figure 14 and Figure 15 present a comparative analysis of the weight of main components between the baseline mGT and

the different mGT-SOFC layouts. For the sake of brevity, results are reported only for systems with take-off as design point.

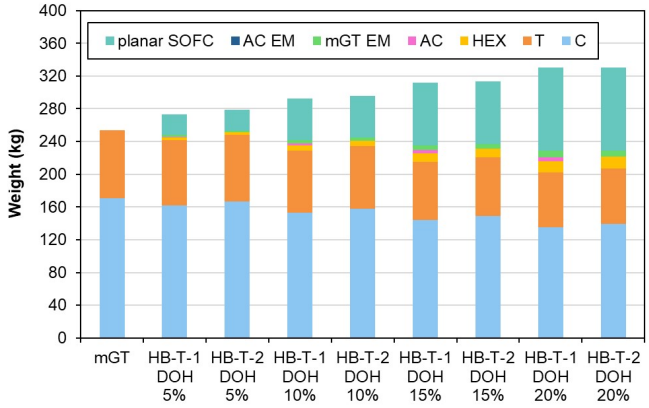

Figure 14: Weight of the main components of each system designed for take-off, assuming planar cells (for this case study).

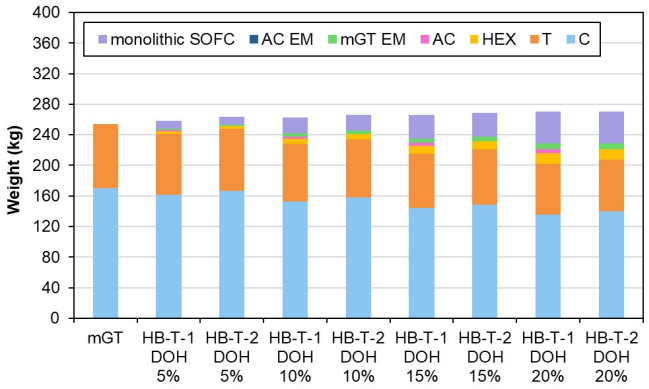

Figure 15: Weight of the main components of each system designed for take-off, assuming monolithic cells (for this case study).

It is important to underline that this is a preliminary analysis, based only on the devices listed in Section 3.4, and therefore the total weight of each layout is underestimated. Moreover, the use of power densities and correlations introduces some uncertainty in the analysis, which could be significantly reduced only by considering the specific geometry and materials of each component. For example, the simplified method does not account for variations in HEX geometry, fin efficiency and flow distribution, as well as density and thermal conductivity, leading to potential deviations in mass estimation. A more detailed analysis of the HEX was carried out to understand the order of magnitude of uncertainty in the results. The HEX was redesigned for the using the core mass velocity approach, with rating and optimization routines [45]. For the layouts HB-T-1 and HB-T-2 and a DOH of 15%, the HEX masses were calculated to be equal to 11.3 kg and 12.3 kg, against the 10.4 kg obtained with the simplified approach.

However, the results presented in this section are valuable to assess how the weight of mGT-SOFC systems increases with the DOH and to understand if this can represent a limitation for their adoption as propulsion systems on aircrafts. Systems based on planar cells are identified by the letter "P", while those based on monolithic cells by the letter "M".

The results show that, given the heavy weight of SOFCs, the mass of the system grows for higher DOH. For DOH = 20%, an mGT-SOFC system based on planar cells would have a +30.2% increase of total mass compared to the baseline H_2 mGT. However, the adoption of the most innovative lightweight technologies, such as monolithic cells, would make it possible to achieve a total mass of the system comparable to the baseline mGT, even for the highest DOH (+6.6%).

The results make it clear that the identification of the mGT-SOFC system design depends on the limitations of the aircraft in terms of weight. Even if, for the specific case evaluated, a higher DOH is a better choice in terms of efficiency, additional hydrogen supply, specific power and steam generation for NO_X reduction, it comes at the cost of a higher weight, which could be unfeasible depending on the SOFC technology. Therefore, the development of lightweight SOFC technology appears to be a key requirement for the adoption of highly efficient mGT-SOFC systems in the aviation industry, which could guarantee higher efficiencies and lower NO_X emissions compared to H_2-fuelled mGTs.

4.3. Sensitivity analysis

Finally, a sensitivity analysis was carried out to understand how the uncertainties on the most relevant performance parameters (polytropic efficiency of compressor and turbine η_{poly}, heat exchanger heat losses Q_{loss}, SOFC pressure losses Δp_{SOFC}) might impact the reliability of the results obtained following the proposed methodology. In particular, variations of net power P_{net}, net efficiency η_{net} and SOFC cathode inlet temperature $T_{in,SOFC,cat}$ were analysed. Referring to an input of the model x, its deviations from the nominal point are defined as $x^+ = x + \Delta x$ and $x^- = x - \Delta x$. The corresponding variations of an output y are represented as y^+ and y^-. The deviations from the nominal point were set as $\Delta\eta_{poly} = 1.0\%$, $\Delta Q_{loss} = 0.5\%$, $\Delta p_{SOFC} = 0.5\%$.

In order to compare the effect of different parameters, non-dimensional sensitivity S is computed according to Eq. (19).

$$S = \frac{(y^+ - y^-)}{(x^+ - x^-)} \frac{x_{nom}}{y_{nom}} \tag{19}$$

Since these input parameters are considered here as uncertainties, the design of each layout is not modified after introducing any deviation Δx. The results are displayed in Figure 16, Figure 17 and Figure 18.

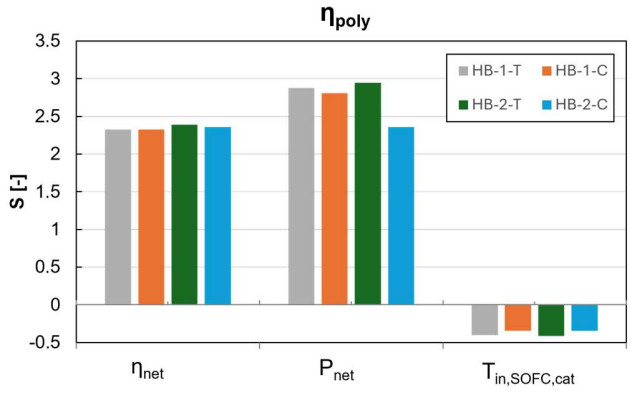

Figure 16: Non-dimensional sensitivity of η_{poly}.

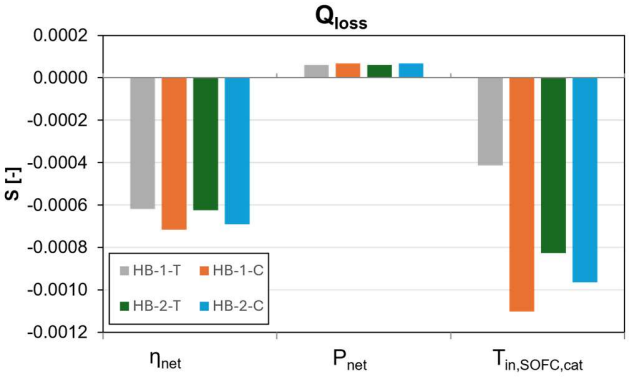

Figure 17: Non-dimensional sensitivity of Q_{loss}.

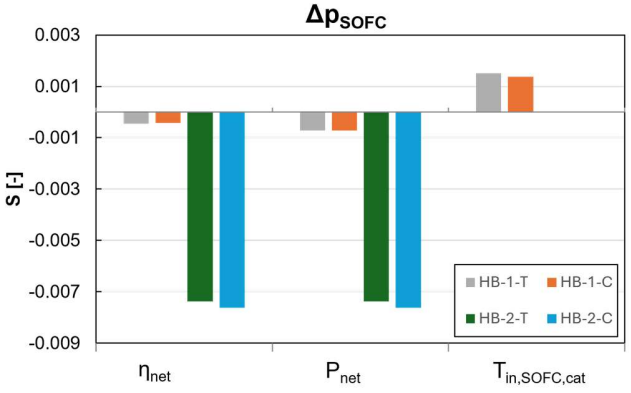

Figure 18: Non-dimensional sensitivity of Δp_{SOFC}.

It is evident that the most impactful parameter is η_{poly}, which has a strong influence on the net power and efficiency of the mGT-SOFC system. Moreover, a higher η_{poly} leads to a lower compressor outlet temperature and consequently to a reduction of cathode inlet air temperature. Therefore, η_{poly} must be accurately estimated before finalizing the design the system.

ΔQ_{loss} is the parameter with the lowest values of sensitivity. Its effect is mainly on the cathode air temperature, since less heat can be transferred to it by the HEX, and on η_{net}, because part of the energy provided by the fuel is dissipated. Since the system adjusts the $\dot{m}_{H2,in,CC}$ to achieve the correct turbine inlet temperature, the influence on P_{net} is negligible.

Δp_{SOFC} is the only parameter with an effect that is significantly different between the HB-1 and HB-2 layouts, even if its impact is generally modest. In HB-1 the AC compensates for any pressure loss in the SOFC circuit. Therefore, the effect of Δp_{SOFC} is very limited, reducing slightly η_{net} and P_{net} because of the increased power consumption of the AC, and increasing the $T_{in,SOFC,cat}$ because of the higher pressurization. On the other hand, increasing the Δp_{SOFC} drives the turbine inlet pressure down in the HB-2, reducing both η_{net} and P_{net}. Since the AC is not present in this layout, the $T_{in,SOFC,cat}$ is not affected.

5. CONCLUSIONS

This article presented a methodology to design, analyze and compare different mGT-SOFC systems for aeronautical applications, considering a hydrogen-fuelled mGT as baseline. To demonstrate the effectiveness of this approach, the case study of an mGT-SOFC was considered, targeting ~955 kW of power at take-off and ~410 kW at cruise. Two different layouts have been proposed for the SOFC system, one with an auxiliary compressor on the SOFC air path (HB-1), and one with an expansion valve on the mGT air path (HB-2). Each layout was considered in multiple variants, designed for take-off or cruise, and with DOH between 5% and 20%.

Simulations on this explorative case study, carried out with the W-TEMP software, showed that mGT-SOFC systems have a better performance than the mGT in terms of net efficiency. This is possible thanks to the much higher efficiency of the SOFC and becomes particularly evident for high DOHs. Thanks to the higher operative pressure of SOFC and turbine, the HB-1 appears as a more performing solution than the HB-2, having about +1% of net efficiency in all designs and exceeding the mGT efficiency by about 5% for DOH = 20%. A higher DOH increases also the amount of hydrogen and water available at the cathode outlet, reducing the amount of additional fuel to be provided at the combustor and offering the potential to reduce NOx emissions.

Regarding the differences between systems designed with take-off or cruise as design point, it is not possible to draw conclusions on the better choice at this stage. In fact, differences in the results are due to changes of ambient pressure and temperature; however, it is necessary to keep in mind that any system, whether it is designed for cruise or take-off, will operate in both conditions during a complete flight mission. Therefore, it will be possible to assess the advantages of one design over the other only after a detailed off-design analysis.

A preliminary estimate on the mass of each configuration of this explorative case study showed that a higher DOH comes at the cost of an increased weight. In fact, the SOFC is a very bulky component, which drives the overall weight of the system up.

Considering only innovative lightweight technologies, two different values of power density were used for SOFCs: 1.88 kW/kg for a stack of planar cells and 4.60 kW/kg for one of monolithic cells. These results highlighted that the adoption of lighter cells makes it possible to limit the weight increase, with differences of just 6.6% in the case of monolithic cells at DOH = 20%.

Finally, a sensitivity analysis on the most relevant performance parameters showed that the polytropic efficiency of compressor and turbine has the most significant effect on the system performance. Therefore, it will be critical to minimize the uncertainty on η_{poly} before finalizing the design of the mGT-SOFC system.

In conclusion, this study presented a comprehensive methodology to design, analyze and compare different mGT-SOFC systems, considering both their performance and weight. The application of this methodology for a specific case study showed that the adoption of mGT-SOFC systems on aircrafts can lead to significant advantages, including higher efficiency, specific power and water generation. However, increasing the size of the SOFC has a significant impact on the weight of the system, and the final design of the mGT-SOFC should be a trade-off between performance and power density, depending on the specific limitations of the aircraft.

Future activities will focus on estimating more precisely the weight of each mGT-SOFC layout and to define the optimal configuration. Then, the results of the layout exploration will be the starting point for many new research activities, including off-design analyses, design and optimization of components, transient simulations and control design. The methodology presented in this paper will help the design of integrated SOFC systems for aviation, such as the +1 MW IPPS of the FlyECO project, which are expected to offer a pathway towards a more efficient and sustainable aviation sector.

ACKNOWLEDGEMENTS

This project has received funding from the European Union's Horizon Europe research and innovation programme under grant agreement No 101138488 and by the UK Research and Innovation (UKRI) funding guarantee under the project reference 10106893. Views and opinions expressed are however those of the author(s) only and do not necessarily reflect those of the European Union, UKRI or CINEA. Neither the European Union nor the granting authorities can be held responsible for them.

Special thanks to S. Bhapkar, Dr. M. Salazar, Prof P. Laskaridis, and Dr. J. Zanger for fruitful discussions, which greatly improved the quality of the present manuscript.

BIBLIOGRAPHY

[1] Publications Office of the European, 2022, *Fly the Green Deal - Europe's Vision for Sustainable Aviation*.

[2] US Federal Aviation Administration, 2022, *FAA Aerospace Forecast FY 2022-2042 | Federal Aviation Administration*.

[3] Meyer, P., Lück, S., Goeing, J., and Friedrichs, J., 2024, "Evaluation of Air Supply Conditioning Architectures for PEM Fuel Cell Systems in Aviation."

[4] Long, D., Wen, H., Shao, Y., and Shuai, Z., 2024, "Evolution and Comparison of Three Typical Permanent Magnet Machines for All-Electric Aircraft Propulsion," Electr. Eng., **106**(3), pp. 2219–2231.

[5] Adu-Gyamfi, B. A., and Good, C., 2022, "Electric Aviation: A Review of Concepts and Enabling Technologies," Transp. Eng., **9**, p. 100134.

[6] Tiwari, S., Pekris, M. J., and Doherty, J. J., 2024, "A Review of Liquid Hydrogen Aircraft and Propulsion Technologies," Int. J. Hydrogen Energy, **57**, pp. 1174–1196.

[7] Guiberti, T. F., Pezzella, G., Hayakawa, A., and Sarathy, S. M., 2023, "Mini Review of Ammonia for Power and Propulsion: Advances and Perspectives," Energy and Fuels, **37**(19), pp. 14538–14555.

[8] Boretti, A., 2024, "Towards Hydrogen Gas Turbine Engines Aviation: A Review of Production, Infrastructure, Storage, Aircraft Design and Combustion Technologies," Int. J. Hydrogen Energy, **88**, pp. 279–288.

[9] Schröder, M., Becker, F., and Gentner, C., 2024, "Optimal Design of Proton Exchange Membrane Fuel Cell Systems for Regional Aircraft," Energy Convers. Manag., **308**, p. 118338.

[10] Campanari, S., Manzolini, G., Beretti, A., and Wollrab, U., 2008, "Performance Assessment of Turbocharged Pem Fuel Cell Systems for Civil Aircraft Onboard Power Production," J. Eng. Gas Turbines Power, **130**(2).

[11] Santin, M., Traverso, A., and Massardo, A., 2008, "Technological Aspects of Gas Turbine and Fuel Cell Hybrid Systems for Aircraft: A Review," Aeronaut. J., **112**(1134), pp. 459–467.

[12] Guida, D., and Minutillo, M., 2017, "Design Methodology for a PEM Fuel Cell Power System in a More Electrical Aircraft," Appl. Energy, **192**, pp. 446–456.

[13] Marinaro, G., Di Lorenzo, G., and Pagano, A., 2022, "From a Battery-Based to a PEM Fuel Cell-Based Propulsion Architecture on a Lightweight Full Electric Aircraft: A Comparative Numerical Study," Aerosp. 2022, Vol. 9, Page 408, **9**(8), p. 408.

[14] Schröder, M., Becker, F., Kallo, J., and Gentner, C., 2021, "Optimal Operating Conditions of PEM Fuel Cells in Commercial Aircraft," Int. J. Hydrogen Energy, **46**(66), pp. 33218–33240.

[15] Baldi, F., Wang, L., Pérez-Fortes, M., and Maréchal, F., 2019, "A Cogeneration System Based on Solid Oxide and Proton Exchange Membrane Fuel Cells with Hybrid Storage for Off-Grid Applications," Front. Energy Res., **6**, p. 419995.

[16] Ferrari, M. L., Traverso, A., Magistri, L., and Massardo, A. F., 2008, "Control System for Solid Oxide Fuel Cell Hybrid Systems," *Proceedings of the ASME Turbo Expo*, American Society of Mechanical Engineers Digital Collection, pp. 55–63.

[17] Brinson, T. E., Ordonez, J. C., and Luongo, C. A., 2012, "Optimization of an Integrated SOFC-Fuel Processing System for Aircraft Propulsion," J. Fuel Cell Sci. Technol., **9**(4).

[18] Xin, T., Wang, Y., and Shi, Y., 2021, "Sizing Design and Simulation of an SOFC Propulsion System for Unmanned Aerial Vehicles," ECS Trans., **103**(1), pp. 785–795.

[19] Singh, M., Zappa, D., and Comini, E., 2021, "Solid Oxide Fuel Cell: Decade of Progress, Future Perspectives and Challenges," Int. J. Hydrogen Energy, **46**(54), pp. 27643–27674.

[20] Ferrari, M. L., Mantelli, L., and Pascenti, M., 2025, "Emulation Tests of Dynamics and Control for a Turbocharged SOFC System," Appl. Therm. Eng., **258**, p. 124514.

[21] Kojima, T., and Okai, K., 2023, "Investigation of Weight and Flight-Path Constraints on Liquid Hydrogen Fueled SOFC/GT Hybrid Propulsion System," AIAA SciTech Forum Expo. 2023.

[22] "Fly-ECO Project Website" [Online]. Available: https://flyeco-european-project.eu/. [Accessed: 03-Dec-2024].

[23] San Benito Pastor, D., Pontika, E., de Graaf, S., Ewald, D., Weber, A., Kazula, S., Ferrari, M. L., and Laskaridis, P., 2025, "Hydrogen-Powered Integrated Power and Propulsion System (IPPS) Architecture for Sustainable Aviation: Leveraging Synergies Between Gas Turbine and Solid Oxide Fuel Cells," Towards Sustainable Aviation Summit (TSAS), Toulouse, France, January 28-30.
DOI: doi.org/10.60711/TSAS25.20250220.7778288272160048. [Accessed: 25-Feb-2025].

[24] Massardo, A. F., and Lubelli, F., 2000, "Internal Reforming Solid Oxide Fuel Cell-Gas Turbine Combined Cycles (IRSOFC-GT): Part A- Cell Model and Cycle Thermodynamic Analysis," J. Eng. Gas Turbines Power, **122**(1), pp. 27–35.

[25] Ortuno, M. S., Yin, F., Rao, A. G., Vos, R., and Proesmans, P. J., 2023, "Climate Assessment of Hydrogen Combustion Aircraft: Towards a Green Aviation Sector," AIAA SciTech Forum Expo. 2023.

[26] Bai, M., Yang, W., Yan, J., Zhang, R., and Qu, Z., 2024, "Cryogenic Turbo-Electric Hybrid Propulsion System with Liquid Hydrogen Cooling for a Regional Aircraft," Int. J. Hydrogen Energy, **71**, pp. 541–561.

[27] McPhail, S., Leto, L., and Boigues-Muñoz, C., 2013, *The Yellow Pages of SOFC Technology*.

[28] Ji, Z., Qin, J., Cheng, K., Liu, H., Zhang, S., and Dong, P., 2021, "Design and Performance of a Compact Air-Breathing Jet Hybrid-Electric Engine Coupled With Solid Oxide Fuel Cells," Front. Energy Res., **8**, p. 613205.

[29] Nehter, P., Geisler, H., Ahilan, V., Friedl, S., Rohr, O., Walter, A., Metzner, C., and Zimmermann, K., 2023, "Solid Oxide Fuel Cells for Aviation," ECS Trans., **111**(6), p. 143.

[30] Collins, J. M., and McLarty, D., 2020, "All-Electric Commercial Aviation with Solid Oxide Fuel Cell-Gas Turbine-Battery Hybrids," Appl. Energy, **265**, p. 114787.

[31] Göke, S., and Paschereit, C. O., 2012, "Influence of Steam Dilution on NOx Formation in Premixed Natural Gas and Hydrogen Flames," 50th AIAA Aerosp. Sci. Meet. Incl. New Horizons Forum Aerosp. Expo.

[32] Traverso, A., Massardo, A. F., Cazzola, W., and Lagorio, G., 2008, "WIDGET-TEMP: A Novel Web-Based Approach for Thermoeconomic Analysis and Optimization of Conventional and Innovative Cycles," Proc. ASME Turbo Expo 2004, **7**, pp. 623–631.

[33] Achenbach, E., 1994, "Three-Dimensional and Time-Dependent Simulation of a Planar Solid Oxide Fuel Cell Stack," J. Power Sources, **49**(1–3), pp. 333–348.

[34] Santin, M., Traverso, A., Magistri, L., and Massardo, A., 2010, "Thermoeconomic Analysis of SOFC-GT Hybrid Systems Fed by Liquid Fuels," Energy, **35**(2), pp. 1077–1083.

[35] Santin, M., and Traverso, A., 2009, "SOLID OXIDE FUEL CELL AND GAS TURBINE HYBRID SYSTEMS FOR AIRCRAFT," *22nd International Conference on Efficiency, Cost, Optimization Simulation and Environmental Impact of Energy Systems*, Foz do Iguaçu, Paraná, Brazil.

[36] Aguiar, P., Adjiman, C. S., and Brandon, N. P., 2004, "Anode-Supported Intermediate Temperature Direct Internal Reforming Solid Oxide Fuel Cell. I: Model-Based Steady-State Performance," J. Power Sources, **138**(1–2), pp. 120–136.

[37] Bessette, N. F., 1994, "Modeling and Simulation for Solid Oxide Fuel Cell Power Systems."

[38] Harvey, S. P., and Richter, H. J., 1994, "Gas Turbine Cycles With Solid Oxide Fuel Cells—Part I: Improved Gas Turbine Power Plant Efficiency by Use of Recycled Exhaust Gases and Fuel Cell Technology," J. Energy Resour. Technol., **116**(4), pp. 305–311.

[39] Kurzke, J., 2002, "Performance Modeling Methodology: Efficiency Definitions for Cooled Single and Multistage Turbines," Am. Soc. Mech. Eng. Int. Gas Turbine Institute, Turbo Expo IGTI, **1**, pp. 85–92.

[40] Dubey, A., Sorce, A., and Stathopoulos, P., 2024, "A Comprehensive Thermodynamic Analysis of Gas Turbine Combined Cycles With Pressure Gain Combustion Based on Humphrey Cycle," J. Eng. Gas Turbines Power, **147**(February), pp. 1–39.

[41] Horlock, J. H., Watson, D. T., and Jones, T. V., 2001, "Limitations of Gas Turbine Performance Imposed by Large Turbine Cooling Flows," J. Eng. Gas Turbines Power, **123**(3), pp. 487–494.

[42] Wilcock, R. C., Young, J. B., and Horlock, J. H., 2005, "The Effect of Turbine Blade Cooling on the Cycle Efficiency of Gas Turbine Power Cycles," J. Eng. Gas Turbines Power, **127**(1), pp. 109–120.

[43] Collins, J. M., and McLarty, D., 2020, "All-Electric Commercial Aviation with Solid Oxide Fuel Cell-Gas Turbine-Battery Hybrids," Appl. Energy, **265**, p. 114787.

[44] Tornabene, R., Wang, X. Y., Steffen, C. J., and Freeh, J. E., 2008, "Development of Parametric Mass and Volume Models for an Aerospace SOFC/Gas Turbine Hybrid System," Proc. ASME Turbo Expo, **5**, pp. 135–144.

[45] Bhapkar, S., and Kazula, S., 2024, "Development of a Predictive Model for the Preliminary Design of Heat Exchangers in Electric Aviation."